Journal of Sound and Vibration 437 (2018) 308–324

Contents lists available at ScienceDirect

Journal of Sound and Vibration

journal homepage: www.elsevier.com/locate/jsvi

Experimental investigation of a novel class of self-centring spinal rocking column

Mohammad M. Kashani [a,*], Alicia Gonzalez-Buelga [b], Rachael P. Thayalan [c], Alistair R. Thomas [c], Nicholas A. Alexander [c]

[a] University of Southampton, Faculty of Engineering and the Environment, Southampton, SO17 1BJ, UK
[b] University of Bristol, Dept. of Mechanical Engineering University of Bristol, Bristol, BS8 1TR, UK
[c] University of Bristol, Dept. of Civil Engineering University of Bristol, Bristol, BS8 1TR, UK

ARTICLE INFO

Article history:
Received 18 January 2018
Received in revised form 24 July 2018
Accepted 16 August 2018
Available online 10 September 2018
Handling Editor: Erasmo Carrera

Keywords:
Rocking column
Accelerated bridge construction
Vertebral bridge pier
Backbone curve
Nonlinear dynamics
Frequency response function

ABSTRACT

This paper explores a proof of concept self-centring spinal column concept experimentally. The idea of the system is inspired by the mechanical interaction of the vertebral bones and intervertebral discs in human spine. Experimental tests are undertaken to explore whether a similar bridge pier system could be constructed to withstand seismic dynamic loading in an equally efficient manner. The experimentation is performed on tied (pre-tensioned) wooden blocks (vertebrae) with and without rubber strips between the vertebrae acting as the intervertebral discs. Small-scale test specimens are excited sinusoidally using a small-scale shake table, and the response of the system recorded through triaxial accelerometers attached to the structure. The nonlinear dynamic response and mechanics of the system are then investigated under sinusoidal dynamic excitation. It is found that the integration of intervertebral rubber discs into wooden vertebrae reduces the nonlinearity of the system, and increases the flexibility and damping. The experimental results show that the proposed system can sustain large lateral displacement without any residual deformation after the excitation.

1. Introduction

The modern seismic design practice [1,2] has improved the seismic response of reinforced concrete (RC) structures under earthquake loading when compared to older structures. Nevertheless, destructive damage has been observed in recent large earthquakes, and financial loss due to such events can be devastating [3]. This is the consequence of designing structures for ductility. In other words, structures are designed for a reduced strength to a specific seismic hazard level, and structural components (beams and columns) are prescriptively detailed in their potential plastic hinge locations for ductility. This design methodology, regardless of the section of infrastructure to which it is applied, has led to a decrease in the number of casualties following seismic events but has also led to a marked, post-quake, increase in cost. One of the most popular examples is the Northridge earthquake where there were 57 casualties, but damages were estimated at $50 billion [4]. Additionally, after the Kobe earthquake in 1995 over 100 reinforced concrete columns were demolished, even though they did not collapse, as the residual displacements were so large, that bridges were deemed to be unusable [5]. Despite neither of these

* Corresponding author.
E-mail address: mehdi.kashani@soton.ac.uk (M.M. Kashani).

https://doi.org/10.1016/j.jsv.2018.08.034

Nomenclature

A	Non-dimensional amplitude of ground acceleration [ ]
a_i, b_i	Fourier coefficients of total acceleration response [m/s^2]
d	Column width [m]
F_0	Initial cable pre-tension force [N]
g	Gravitational acceleration constant [m/s^2]
h	Column height [m]
k_c	Cable stiffness [N/m]
k_s	Contact stiffness [N/m^2]
m	Mass of deck [kg]
M	Moment-rotation function [Nm]
q_i	Backbone curve coefficients [1/s, 1/m/s, 1/m^2/s, 1/m^3/s]
x	Relative displacement of top of tower [m]
x_g	Displacement of ground [m]
X_g	Amplitude of ground displacement [m]
X_r	Amplitude of tower displacement [m]
β	Ratio of contact to cable stiffnesses [ ]
γ	Viscous damping ratio [ ]
δ_r	Rocking (rigid body) displacement of tower [m]
δ_f	'Flexural-like' displacement of tower [m]
Δ_{tot}	'Flexural-like' plus rigid body displacement of tower [m]
η	Angle at which joint at bottom of tower open up [rad]
θ	Rotation of bottom of tower [rad]
μ	Non-dimension moment-rotation function [ ]
μ_k	Friction coefficient for Coulomb damping model [ ]
ξ	Damping function [1/s]
Π	Lagrangian [Nm]
φ	Non-dimension rotation at bottom of tower [ ]
ω_0	Fundamental natural system frequency [rad/s]
ω_r	Excitation frequency of ground motion [rad/s]
ω	Nonlinear resonant frequency [rad/s]
Ω	Ratio of excitation to natural frequency [ ]
ψ	Dimensionless simplification variable (function of β and ϕ)

cases occurring within the purview of modern seismic design code [1,2], it is the same design approach that has led to a lack of resilience in the transport sector.

Moreover, there are currently a large number of bridge structures that are located in seismic regions that also suffer from material ageing and reinforcement corrosion [6]. Corrosion reduces the safety margin of these structures, and their residual capacity is much smaller than the original design [7–9]. However, the current state-of-practice in design and construction relies on monolithic construction, which is extremely time consuming and not resilient to environmental stressors such as chloride-induced corrosion and natural hazards such as earthquake. Therefore, there is an urgent need for replacement of vulnerable bridges, and the development of novel and smart structural systems for accelerated bridge construction, that is resilient to environmental stressors and natural hazards.

The motivation for designing a spinal column stems from Accelerated Bridge Construction (ABC). Following this approach, the columns are assembled from precast concrete segments produced off site in a factory. ABC produces a higher quality of concrete due to its manufacture in a controlled environment, where standards are more easily managed. Additionally, it reduces traffic disruption and is less prone to weather delays. Most significantly, the construction time of precast columns is far shorter than a monolithic column, which subsequently reduces the construction costs for large-scale projects [10]. However, currently the use of segmental post-tensioned concrete bridge columns is not very popular in high seismicity regions. The main concern is the seismic performance of these structures and the damage incurred [11].

Lin and Mo [12] tested a series of columns where the hinge segment was monolithically cast at the base of the column with the foundation. They achieved great success with smaller columns as they kept the joint outside of the potential plastic hinge region of the column. However, in large bridges, the payload capacity of trucks transporting precast column segments and the crane to be used in assembling these segments are important limiting factors. Therefore, it is difficult to design the joints to be away from the potential plastic hinge regions, because the height of column segments must be limited to a certain size, due to their weight. Numerous experimental studies conducted to achieve the energy dissipation necessary across these joints to

withstand medium to high seismic activity [13–20]. Arai et al. [13] used continuous steel tubes across the joints, but despite observing small residual displacements, there was also minimal energy dissipation. Hewes and Priestley [14] tested segmental columns with an unbounded tendon design. Unbounded design results in a crack appearing between the structure and the foundation as the column effectively rotates as a rigid body. This results in a substantial compressive strain localisation at the critical section and subsequently crushing of the concrete in compression [14]. Moreover, unbounded design also reduces the possibility of yielding of the tendon, but also decreases the lateral strength of a structure. Other researchers [15,16] have used ductile fibre-reinforced cement-based composites. Some researchers have used the concept of rocking in timber structures in conjunction with energy dissipation devises [17,18]. In all these cases, although damage was minimised, the system was intended to be damage-tolerant, rather than damage-free.

More recently, a hybrid sliding-rocking column was developed by Sideris [21]. This system employs sliding joints to dissipate energy along the length of the column, rather than using energy dissipating links in rocking-only-columns. Duct adaptors span the joints and control the amplitude of sliding. Although the sliding does reduce damage significantly, some wearing at the joint was identified, which require repair after the earthquake.

In all the previous literature (mentioned above), researchers have tried to minimise the residual drift of bridge piers after the earthquake. However, to provide the self-centring mechanism and damping in the structural system, they still allow the bridge pier to sustain some permanent damage after the earthquake. The research presented in this paper explores the development of a novel damage-free structural system, which is inspired by mechanics of the human spine. In the human spine, intervertebral discs of the spine provide flexibility and absorb and transmit loads without damaging the vertebrae bones. Compression of these discs results in strains between 3% and 10% experienced by the annulus fibrosus, the tough exterior of the disc [22]. The proposed proof of concept design is a spinal bridge column concept that is made of wooden blocks (the 'vertebrae'), and thin layers of rubber between the wooden blocks (the 'intervertebral discs'). Finally, individual components are tied together using an unbonded post-tensioning tendon (the 'longitudinal ligament'), which provides a self-centring mechanism in the column when subjected to lateral force. The proposed spinal column employs multiple rocking mechanisms within the bridge column (elastic hinges). As a result, the column will flex and elastically displace laterally (geometrically nonlinear) without damage, unlike conventional RC columns. The self-centring mechanism in the column re-centres the bridge to its original position after any large lateral displacement; i.e. displacements are recoverable and resilient.

In this study, two types of self-centring rocking spinal columns are dynamically tested. One with elastomeric intervertebral discs (IRD) between the vertebrae joints, and another with no intervertebral discs. The aim of this study is to explore the performance of this spinal column system, including energy dissipation, residual displacement and structural capacity under real-time dynamic loading. This is achieved by studying the behaviour of the systems under dynamic load and extracting the nonlinear resonance curves. A shaking table testing protocol is developed to apply real-time dynamic base excitation.

1.1. Experimental programme

There are several different experimental techniques that can be used to study the behaviour of structures under dynamic loading [23]. Shaking table testing provides real-time dynamic base excitation, making it ideal to study seismic loads. Generally, their use is restricted to reduced-scale models, tough a few tables exist which have the capacity to apply seismic base motions to full-scale systems [24]. In this paper, we present experimental results obtained from testing a small-scale spinal rocking column system using an uni-directional shaking table. The shaking table consists of a rigid base mounted on linear bearings and driven by an electromagnetic actuator. The displacement of the base is controlled via a linear variable displacement transducer (LVDT) using Simulink and dSpace [25] as a software platform for experimental control. The proposed test specimen is mounted directly onto the shaking table base, as shown in Fig. 1.

A set of 50 mm square wooden blocks are used to model the '*vertebral body*' in the system, while 5 mm thick rubber layers are used to model the '*intervertebral discs*'. This thickness of rubber represents a ratio of wooden block thickness to elastomeric layer thickness of 10. For a full-scale system, this ratio provides a realistic estimate of the thickness of the elastomeric pad. A hole was drilled into the centre of each block and each rubber layer to allow for a 1 mm diameter, 19 strands, high-strength stainless steel cable to run through the structure. The elastic modulus of the wooden blocks and stainless steel cable are 1.25×10^4 MPa and 1.18×10^5 MPa respectively. Fig. 2 shows the configuration of the structural models tested in this research. To create the inertia force in the system, a 2.5 kg lump mass is added at the top of test specimen and secured in a wooden box (Fig. 2). The self-centring mechanism is provided by the cable with a 300N pre-tensioned force.

Based on previous analysis of rocking systems [26], it was expected the system would behave in a nonlinear manner. It exhibits a nonlinear stiffness softening characteristic with increasing deformation amplitude. In a softening system, the response frequency, of the free-vibrating system, will decrease with increasing amplitude [27]. In other words, the natural frequency of the system is response amplitude dependant.

Following steps defined by Kerschen et al. [28], the nonlinear behaviour of the system under study was first detected, then characterised and finally the nonlinear system's parameters were estimated and compared with a simplified theoretical model. In the model under investigation, several sources of nonlinearity can be identified: (i) geometric nonlinearity, associated with large displacements; (ii) nonlinearity due to the boundary conditions at the joints; (iii) nonlinear material behaviour associated with the rubber inserts.

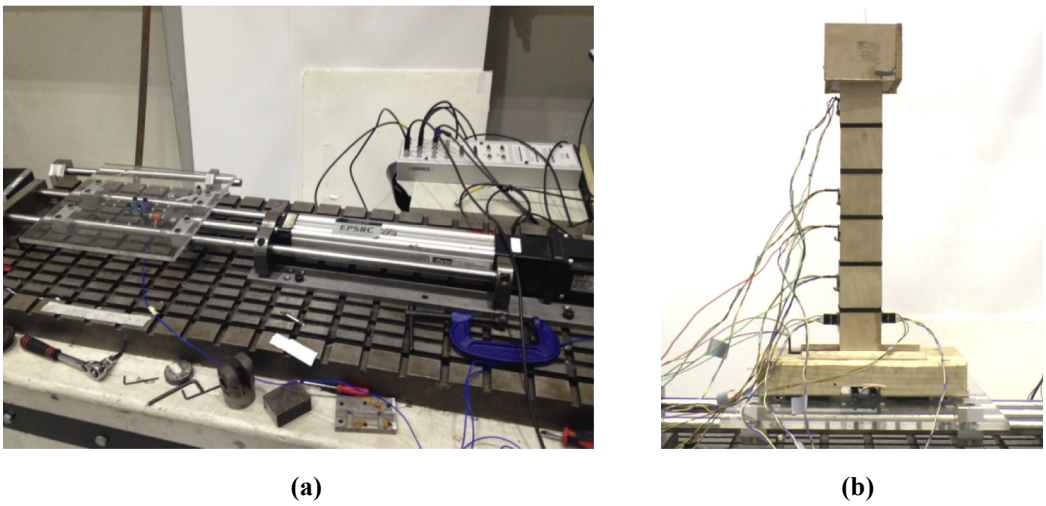

Fig. 1. Experimental test setup: (a) Uniaxial shaking table (b) rocking column specimen mounted on to the shaking table.

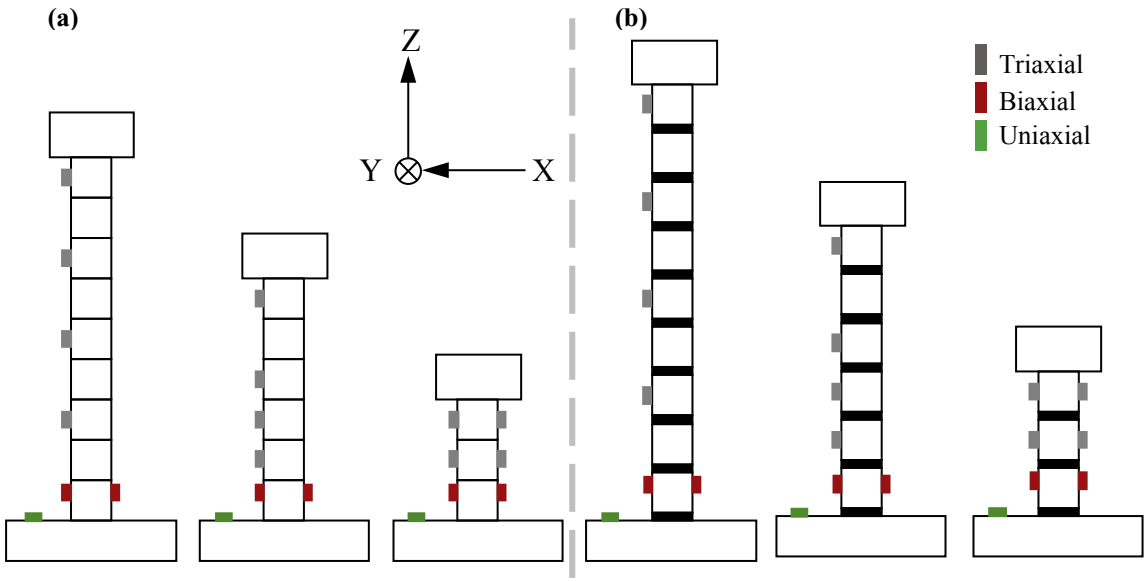

Fig. 2. Experimental scaled models of spinal columns and the locations of the accelerometers: (a) vertebral column without rubber layers, and (b) vertebral columns with rubber layers.

The response of the system is studied in the frequency domain. In structural dynamics, one of the most widely-used methods of visualising the input-output properties of a system is to construct the Frequency Response Function (FRF). There are basically four types of excitation that can be used to study FRFs, such as impulse, stepped-sine, chirp, and random [29]. Stepped-sine produces the more distorted FRFs and this is normally recommended, although it is very time-consuming compared with the other types. Due to the nonlinear nature of the system two key deliberations should to be considered. First, the system must be in steady state (that is transient motions have completely attenuated) before recording the response for a given forcing. Secondly, the frequency steps of the frequency sweep (changing the frequency; i.e. sweep up means increasing frequency and sweep down means decreasing frequency) must be small and smooth enough to ensure the system stays close to the nearest stable solution branch. In the analysis of the experimental results, only the steady state periodic solutions will be presented.

The response of the system is monitored using a total of seven Microelectromechanical System (MEMS) triaxial accelerometers arranged as shown in Fig. 2. Acceleration is measured in the plane of motion of the table (X), out of plane (Y) and in the vertical direction (Z).

2. Experimental results and discussion

2.1. Frequency Response Function (FRF)

In this section we present results from a medium height spinal column with six vertebrae. Several other configurations, with a different number of vertebrae, were tested (Fig. 2) revealing similar qualitative FRFs.

The FRFs are developed by relating base displacement input to relative acceleration output. The signal from the accelerometers shown in Fig. 2 is filtered, in order to remove noise. Since there is an accelerometer located at the base, the relative acceleration can be calculated. The presented FRF (for a given amplitude of base displacement) is computed by estimating the maximum relative acceleration response that is defined here as the mean plus $\sqrt{2}$ times the standard deviation of the measured response history of the system. This represents an unbiased estimate of the peak system response.

Fig. 3 displays the maximum relative accelerations measured at the top of the column, versus base excitation frequency. Fig. 3(a) and (b) shows the response of the system without rubber layers. The dynamic response of the spinal column exhibits a clear softening nonlinearity, which is in good agreement with results reported in Ref. [24]. Due to the nonlinearity, at a certain forcing frequency range, two solutions coexist, one in a lower energy branch while the other belongs to a high energy branch. As it can be seen in Fig. 3(a) and (b), the abovementioned frequency range is quite large (3–6 Hz). This is a very challenging dilemma from the design point of view, i.e. the co-existence of different amplitude stable solutions for a given scenario.

After adding the intervertebral rubber discs (IRD) the dynamics of the system changes. First, in the out of plane motion, there are no longer any multiple solutions observed. Secondly, the inclusion of the IRD considerably reduces the maximum response in both in-plane and out-of-plane motion, by about 40%. Thirdly, the IRD also shifts the resonance curve of the system due to the increased flexibility of the joints. Fourthly, in the plane of the response motion (although there is still signs of co-existing nonlinear softening and stable solutions) the interval of frequency over which this happens is reduced by about 80%. In brief, the addition of the IRD not only minimises the response of the structure but also greatly reduces the challenge of dealing with a multiple solutions scenario.

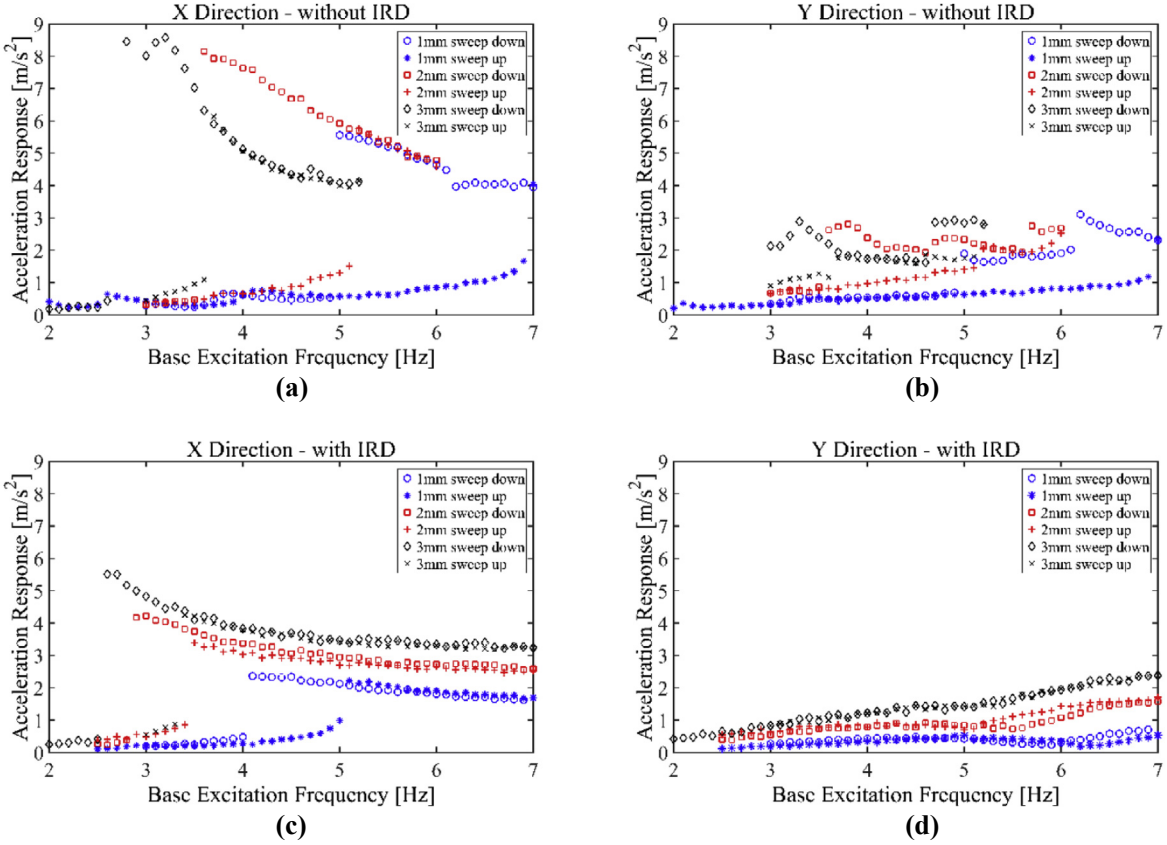

Fig. 3. Frequency response functions for both in plane and out of plane relative acceleration, with and without IRD: (a) FRF in X-direction no IRD, (b) FRF in Y-direction no IRD, (c) FRF in X-direction with IRD, and (d) FRF in Y- direction with IRD.

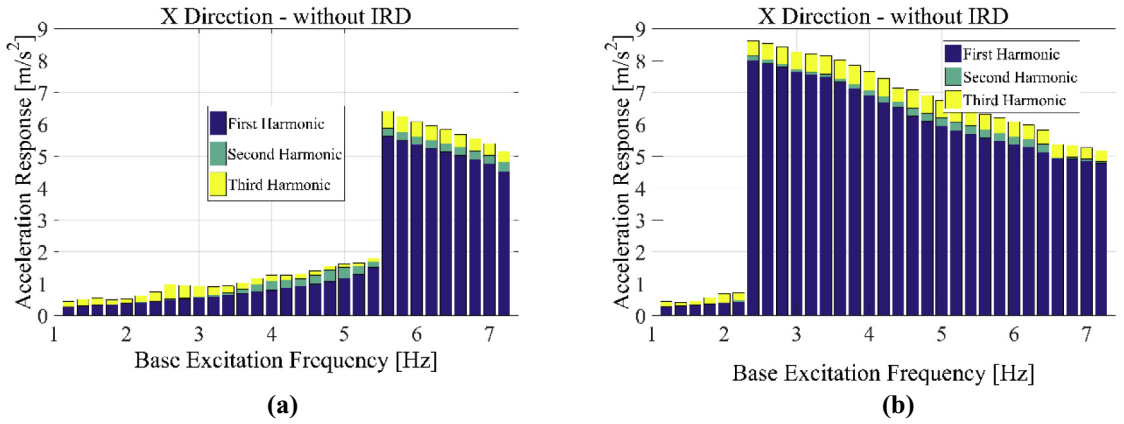

Fig. 4. Frequency content of 6 vertebrae column without IRD at 2 mm amplitude excitation: (a) frequency content of in plane sweep up, (b) frequency content of in plane sweep down.

2.2. Frequency content analysis

Fig. 4 shows the analysis of the frequency content of the recorded acceleration responses. While linear systems respond only at the forcing frequency, the response of nonlinear systems can contain many harmonics. The case presented in Fig. 4, shows the column with six vertebrae, and a sine wave excitation signal. The measured periodic steady-state total acceleration response of the system is expressed as Fourier series, thus

$$\ddot{x} + \ddot{x}_g = \frac{1}{2}a_0 + \sum_{j=1}^{n} a_j \cos(j\omega t) + b_j \sin(j\omega t) \tag{1}$$

The Fourier coefficients a_j and b_j were estimated by using a least squares optimization. It was found that three harmonics, $n = 3$, were sufficient to characterise the response. Fig. 5 shows the frequency content of the rocking column without IRD for both sweep up and down experiments. This pattern is observed in all other undertaken tests.

3. Theoretical analysis

3.1. Reduced-order equation of motion

As discussed in the observed experimental results, the nonlinear response of the column is mainly due to rocking of the first vertebrae. Therefore, it is a reasonable assumption to use a simplified equivalent single degree of freedom (SDOF) model

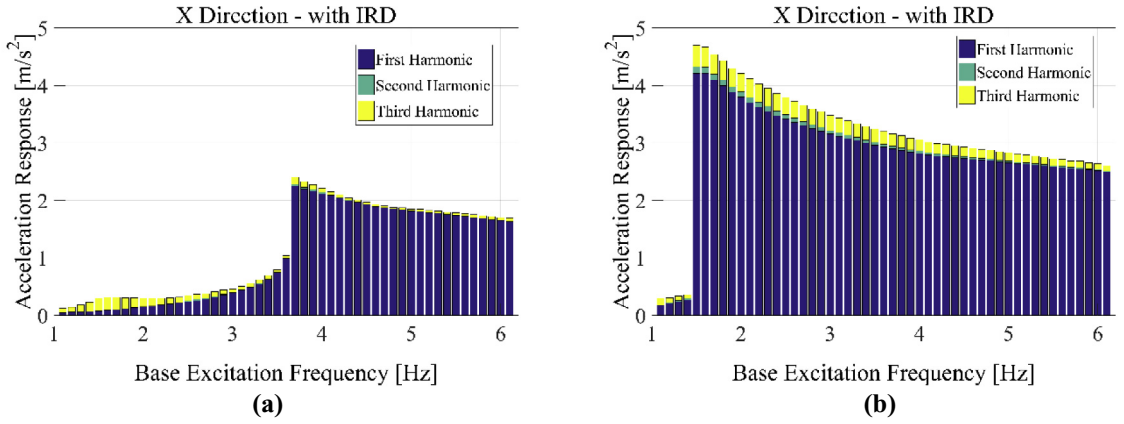

Fig. 5. Frequency content of 6 vertebrae column with IRD at 2 mm excitation amplitude: (a) frequency content in plane sweep up, (b) frequency content in plane sweep down.

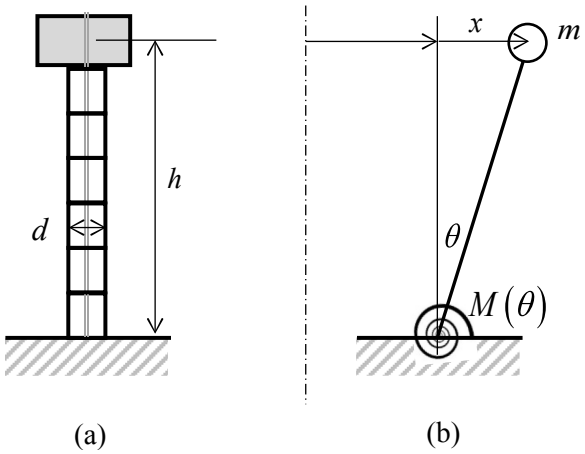

Fig. 6. Idealised reduced-order model: (a) Actual system (b) SDOF equivalent system based on only base rotation.

in the theoretical analysis. The proposed modelling assumptions are shown in Fig. 6 and mathematically explained in this section.

The Lagrangian Π (kinetic minus potential energy) for the equivalent SDOF system above is defined as follows

$$\Pi = \frac{1}{2}m(\dot{x}+\dot{x}_g)^2 - \int M(\theta)\mathrm{d}\theta \tag{2}$$

where m [kg] is the mass of the deck (lumped mass on top pf the column). The assumptions made here are (*i*) column only opens at the base joint (*ii*) large geometrical displacements (second order effect) are neglected (*iii*) the nonlinearity is due to the extension of the pre-tensioned cable and change in contact geometry alone (that is expressed in function $M(\theta)$).

The equivalent system in Fig. 6(b) is very similar to a tied rocking block described in Ref. [26]. Hence introducing non-dimensionalisations from Ref. [26].

$$x = h\eta\varphi, \quad x_g = h\eta\varphi_g, \quad \theta = \eta\varphi, \quad \eta = \frac{2F_0}{d^2k_s}, \quad \beta = \frac{k_s d}{k_c}, \quad M(\theta) = \frac{1}{6}F_0 d\mu(\varphi,\beta) \tag{3}$$

System parameter η is the angle (in radians) at which the base joint opens, it is defined in terms of the cable tension F_0 [N], the vertebra contact stiffness k_s [N/m^2] and the vertebra width d [m]. Parameter β is the ratio of the vertebra contract stiffness to the cable stiffness k_c [N/m]. The moment rotation $M(\theta)$ [Nm] is defined in terms of non-dimensional moment-rotation function $\mu(\varphi,\beta)$ [ ] (see Ref. [24])

$$\mu = \begin{cases} \varphi, & |\varphi| \le 1 \\ \left(\frac{3}{\beta}+\frac{12}{\beta^2}+\frac{8}{\beta^3}\right)\varphi + \left(3+\frac{9}{\beta}+\frac{6-6\sqrt{\psi}}{\beta^2}-\frac{6\sqrt{\psi}}{\beta^3}-\frac{2\psi^{3/2}}{\beta^3\varphi^2}\right)\mathrm{sgn}(\varphi), & |\varphi| > 1 \end{cases} \tag{4}$$

$$\psi = (1+\beta)\left(\varphi^2+\beta|\varphi|\right) \tag{5}$$

Fig. 7 displays the form of the non-dimensional moment-rotation relationship of Eqs. (4) and (5). As a validation, the model is compared with the experimental results from a pushover test of a 9 vertebrae column. Note that the form is very close to the theoretical predictions. Hence Eq. (2) becomes

$$\Pi = \frac{1}{2}mh^2\eta^2(\dot{\varphi}+\dot{\varphi}_g)^2 - \frac{1}{6}F_0 d\eta\int \mu(\varphi,\beta)\mathrm{d}\varphi \tag{6}$$

And therefore, the equation of motion is defined as follows,

$$mh^2\eta^2\ddot{\varphi} + \frac{1}{6}F_0 d\eta\mu(\varphi,\beta) = -mh^2\eta^2\,\ddot{\varphi}_g, \tag{7}$$

Dividing this equation by the generalised mass polar moment of inertia $mh^2\eta^2$, Eq. (7) becomes

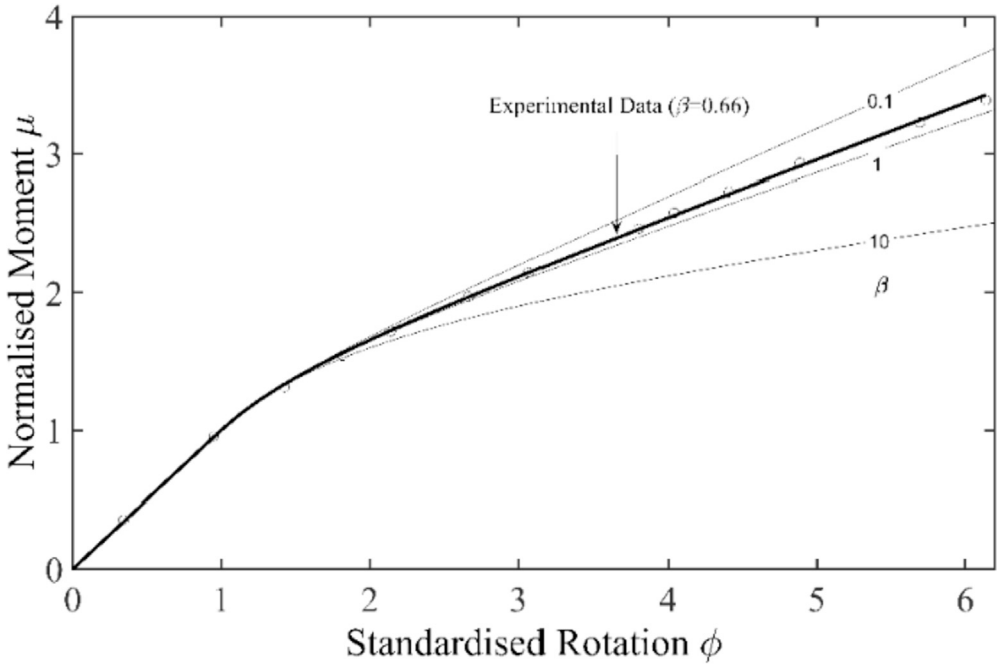

Fig. 7. Normalised nonlinear moment rotation relationship (Eqs. (3) and (4)) with an example of experimental push-over data for 9 block column without rubber.

$$\ddot{\varphi} + \omega_0^2 \mu(\varphi, \beta) = -\ddot{\varphi}_g, \tag{8}$$

The system frequency parameter ω_0 [rad/s] is the linear natural frequency of the system under small vibration, when the base joint does not open. ω_0 is defined as follows,

$$\omega_0^2 = \frac{dF_0}{6mh^2\eta} = \frac{d^3 k_s}{12mh^2} \tag{9}$$

Note that in this theoretical model, the linear natural frequency ω_0 appears mathematically independent of the cable tension F_0. This is if we assume linear contact mechanics, i.e. the contact stiffness k_s is a material/geometric constant. In practice, however, for low normal contact forces and very stiff materials (e.g. steel) the contact stiffness k_s increases as the area of contact increases until a saturation of contact is observed [30]. Consequently k_s may not be exactly constant but a nonlinear function of normal contact force. Therefore, in practice, ω_0 may appear to have some small dependency on the cable tension. By time-scaling $t = \tau/\omega_0$, the equation of motion, Eq. (8) becomes

$$\varphi'' + 2\gamma\varphi' + \mu(\varphi, \beta) = -\varphi''_g, \tag{10}$$

where primes indicate derivatives with respect to scaled time τ; i.e. $\varphi' = \mathrm{d}\varphi/\mathrm{d}\tau$. A damping function $2\gamma\varphi'$ is introduced to account for energy losses. The experimental base excitation is defined (using displacement control) as follows,

$$x_g = X_g \cos(\omega_r t) \tag{11}$$

Therefore, the relationship between the dimensional ground (base) displacement amplitude X_g and the non-dimensional amplitude parameter A is given as follows,

$$-\varphi''_g = A\cos(\Omega\tau), \quad A = \frac{X_g}{h}\frac{\Omega^2}{\eta}, \quad \Omega = \frac{\omega_r}{\omega_0} \tag{12}$$

Eq. (10) is defined in terms of the minimum set of system parameters, that is γ and β plus excitation parameters A and Ω.

3.2. Nonlinear back-bone curves

The backbone curves are the most important characteristics of any nonlinear system [28–31]. Rosenberg [32] extended modal analysis of linear systems to nonlinear systems, and defined the concept of nonlinear normal mode (NNM). Nonlinear modes can be synthesised when a harmonic input cancels out the damping forces. As a result, they form the backbone of the system and they approximate the behaviour of the system at resonance, when a system is a greater risk of failure [28,33].

Equation of motion (Eq. (10)) is obtained from physical reasoning and identifies key non-dimensional parameters of the system. However the complexity of the moment rotation relationship, Eq. (4) does not allow a relatively straightforward estimation of the nonlinear back-bone curves of the system. If expressions in Eq. (4) are approximated by a low-order odd polynomial (series) expansion, then the dimensional form of the equation of motion, Eq. (10), can be estimated as follows,

$$\ddot{x} + \xi(\dot{x})\dot{x} + \omega(x)x = -\ddot{x}_g \tag{13}$$

$$\omega(x) = q_1 + q_2 x + q_3 x|x| + q_4 x^3 \tag{14}$$

An approximation of the experimental FRFs is going to be developed by using the harmonic balance method. Harmonic balance assumes that the response to a sinusoidal excitation is a sinusoid at the same frequency. The objective of this model is to use the measured response data to derive the forms of the amplitude dependant natural frequency $\omega(x)$. For this analysis it is assumed that the damping function is $\xi(\dot{x}) = 2\gamma\omega_0$.

Let the excitation and response of the system be approximated by the following,

$$-\ddot{x}_g = A\cos(\omega_r t + \phi),\ x = X_r\cos(\omega_r t) \tag{15}$$

These values are substituted into Eq. (13), and the procedure described in Ref. [29] is followed to estimate the amplitude dependant natural frequency parameters. The $|x|$ term can be expressed in terms of the signum function, $\mathrm{sgn}(x) = |x|/x$, whose Fourier series expansion can be calculated using the following

$$sgn(\sin(\omega_r t)) = \frac{4}{\pi}\sum_{k\in\mathbb{Z}_{even}}\frac{1}{k}\sin(2k\omega_r t),\quad \mathrm{sgn}(\cos(\omega_r t)) = \frac{4}{\pi}\sum_{k\in\mathbb{Z}_{odd}}\frac{(-1)^{(k-1)/2}}{k}\cos(k\omega_r t) \tag{16}$$

Hence, substituting Eqs. (15) and (16) into equation of motion, Eq. (13), and then balancing only those terms at the primary system resonance results in two equations for the coefficients of $\sin(\omega_r t)$ and $\cos(\omega_r t)$ thus,

$$\begin{aligned} -\omega_r^2 X_r + q_1 + \frac{8}{3\pi}q_2 X_r + \frac{3}{4}q_3 X_r^2 + \frac{25}{12\pi}q_4 X_r^3 &= A\sin\phi \\ -2\gamma\omega_0\omega_r X_r &= A\cos\phi \end{aligned} \tag{17}$$

At resonance, that is assumed to be a point belonging to the backbone curve, the excitation harmonic force $-\ddot{x}_g$, and the harmonic response x are in phase, i.e. $\phi = 0$, with the damping force in quadrature. Solving for ω_r and A, the response frequency, ω_r, is a function of excitation amplitude X_r, thus

$$\omega_r^2 = q_1 + \frac{8}{3\pi}q_2 X_r + \frac{3}{4}q_3 X_r^2 + \frac{25}{12\pi}q_4 X_r^3 \tag{18}$$

Eq. (18) is the numerical approximation for the backbone curve of the nonlinear system, where q_k factors are fitting coefficients. Note that it is most accurate for small X_r. This study is focused on harmonic solutions, therefore the modulus of the displacement response is $X_r = \omega_r^2\sqrt{a_1^2 + b_1^2}$ were a_1 and b_1 are the first harmonic (Fourier) components of the recorded acceleration response, see Eq. (1)

3.3. Experimental backbone curves and nonlinear damping models

Fig. 8 shows the comparison of the numerical backbone curve (Eq. (18)) with the observed experimental results of the 1st harmonic. Fig. 8(a) and (b) compares the numerical backbone curve using Eq. (18) to the experimental sweeps. Fig. 8(c) and (d) compares the numerical and experimental sweep together with the numerical backbone curve for 1 mm amplitude sweep down ground motion excitation.

At resonance, the response of the system and the excitation are in phase, with the damping in quadrature; therefore from Eq. (17) at $\phi = 0$, it follows that,

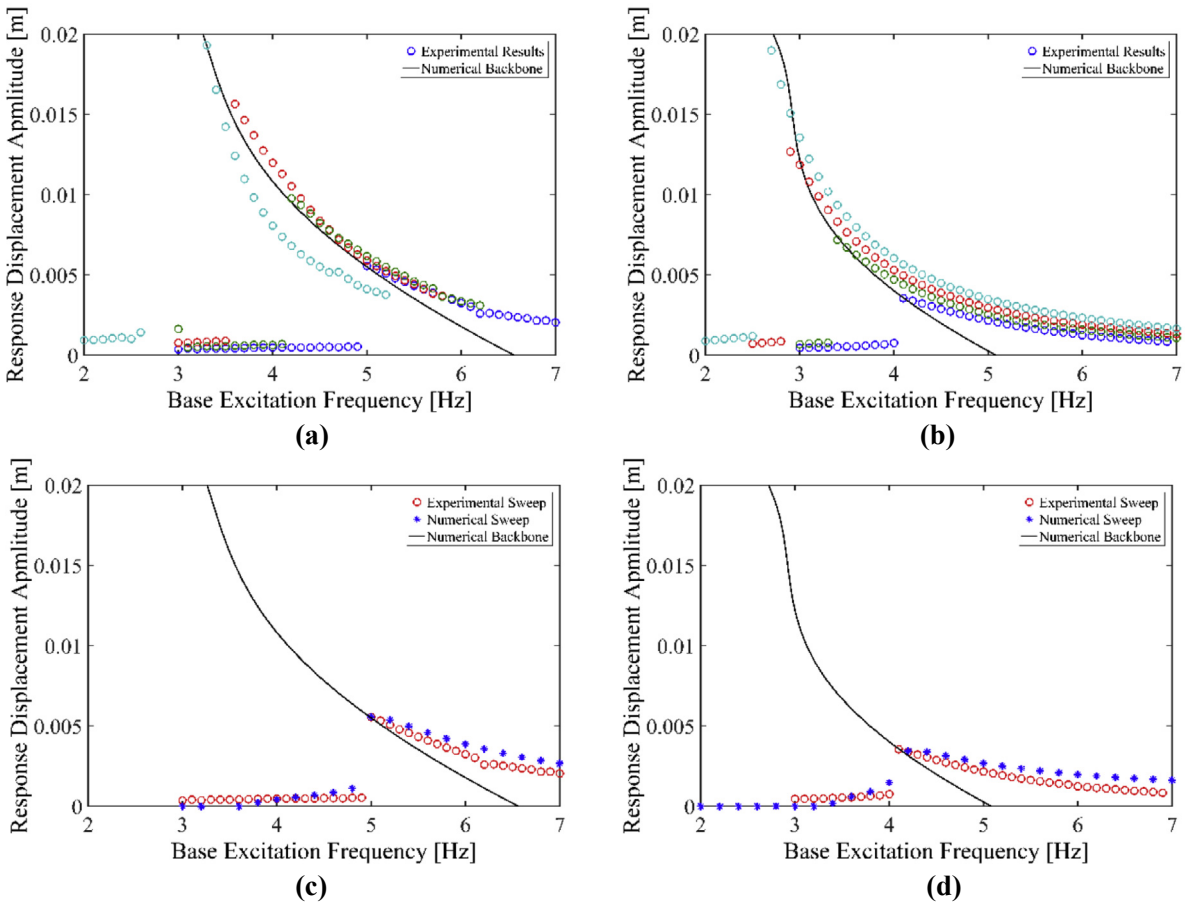

Fig. 8. Comparison of experimental results and numerical simulations: (a) and (b) experimental sweeps and numerical backbone curve [(a) without IRD, and (b) with IRD], and (c) and (d) experimental and numerical sweeps and numerical backbone curve [(c) without IRD, and (d) with IRD].

Table 1
Fitted coefficient of the numerical model in Eq. (18).

Parameter	q_1	q_2	q_3	q_4
Without IRD	1.7×10^3	-2×10^5	1.1×10^7	-2.1×10^8
With IRD	1×10^3	-1.5×10^5	1×10^7	-2.7×10^8

$$\gamma = \frac{1}{2}\frac{\omega_r}{\omega_0}\frac{X_g}{X_r},\ X_g = \frac{A}{\omega_r^2} \tag{19}$$

where ω_r is the excitation frequency, ω_0 is the linear (very small amplitude) natural frequency, X_r is the amplitude of the periodic structural response, and X_g is the ground motion displacement amplitude (see Table 1).

Table 2 gathers the identified damping parameters. Note that in this case the damping depends on the level of ground acceleration. This level corresponds to excitation displacement amplitudes X_g of 1, 1.5, 2, and 3 mm at the resonant frequency of each point of the backbone.

From Table 2, it is evident that adding the IRD increases the damping of the system by about 30%. It is also shown that the damping values depend on the level of forcing. Larger values of damping correspond to low energy input, which is for smaller displacements. This is evidence suggestive of dry friction in the system. Therefore, our damping model is further refined by including nonlinear, Coulomb damping. This is due to the sliding if vertebrae against each other and some sliding of the cable in the hole between the blocks. This is a very important finding and is a key factor in the development of smart civil engineering structures (e.g. bridge piers) in seismic regions. Hence, we consider a combined viscous and Coulomb damping model of the following form,

Table 2
Numerical model identified parameters for the linear damping model.

Ground displacement amplitude X_g	1 mm	1.5 mm	2 mm	3 mm
γ without IRD	0.0723	0.0516	0.0361	0.0258
γ with IRD	0.1148	0.0696	0.0474	0.0379

Table 3
Experimentally estimated values of nonlinear damping parameters.

	γ	μ_k
Without IRD	0.0258	0.051
With IRD	0.0379	0.036

$$\xi(\dot{x})\dot{x} = 2\gamma\omega_0\dot{x} + \mu_k g \mathrm{sgn}(\dot{x}) \tag{20}$$

The viscous damping will be dominant when the velocity of the response, $\dot{x}$, is high, while the dry friction will be dominant for slow quasi-static response motion. Applying this, the damping terms are estimated independently in two steps, firstly μ_k and secondly γ. To estimate the dry friction coefficient μ_k low frequency and low amplitude testing was performed, such that $|\dot{x}| < \varepsilon$ and the damping term is dominated by friction. The viscous damping coefficient γ is estimated from fast response records (high frequency tests). These two initial estimations are iterated to adjust the numerical model to the experimental results over all frequency range. The estimated values are shown in Table 3.

For the purposes of experimental comparisons, Eq. (10) is re-expressed in dimensional form, with viscous and Coulomb damping, as follows,

$$\ddot{x} + 2\gamma\omega_0\dot{x} + \mu_k g\ \mathrm{sgn}(\dot{x}) + \omega_0^2 h\eta\mu\left(\frac{x}{h\eta}, \beta\right) = -\ddot{x}_g \tag{21}$$

Fig. 9 shows the comparison of the nonlinear resonance curve of Eq. (21) with experimental data of a 6 vertebrae column without IRD. A qualitatively good match is obtained, suggesting that the low-order model, Eq. (21), is a reasonable approximation for this system. The mismatch for the high amplitude upper branch of the nonlinear resonance curve is suggestive of amplitude (displacement) dependant damping. A more sophisticated damping model will be explored in future publications.

3.4. Nonlinear dynamic moment-rotation behaviour

As explained earlier, the plastic moment and rotation capacity are the most important parameters governing the seismic performance of bridge piers. Therefore, in this section the nonlinear moment-rotation behaviour of the system is explored. Rotation of the structure can be approximated by deriving the rotation of the bottom vertebra, θ (Fig. 10). Assuming an equivalent SDOF system (Fig. 6), the rotation of the whole structure can be approximated. The SDOF system assumes the whole spinal column is rocking about the edge of the bottom vertebra, and the rest of the structure is rigid. Therefore, θ can be found using simple trigonometry as shown in Fig. 10. The Δ_z is the change in displacement calculated from comparing the accelerometer data recorded from A5 and A6, and d is the column width.

The moment-rotation hysteretic loops of the 9 vertebrae systems with and without IRD are shown in Fig. 11. As expected, the moment-rotation curves show a linear region, where the joints do not open, and a nonlinear region, where the joints open on both sides of the vertebrae [26]. The column without IRD rocks at the first joint and behaves like an inverted pendulum. However, when IRD is added to the system, the friction between the segments increases. Furthermore, rubber by nature is a nonlinear viscoelastic material. Therefore, it deforms and changes the rocking mechanism. The system without IRD is essentially a tied rigid rocking block problem, but the system with IRD is a multiple rigid rocking blocks with nonlinear interfaces system. As a result, although the system is more flexible, but the response is reduced in the column with IRD due to adding the material nonlinearity, increased friction and subsequently increased damping. This is in good agreement with conclusions reported in Ref. [34]. However, overall these curves show a small level of hysteretic energy dissipation.

Fig. 12 shows a comparison of the experimental dynamic moment-rotation graph and the numerically obtained quasi-static and dynamic moment-rotation graphs using solutions of Eq. (21). Note that the experimental results show some asymmetrical behaviour which is due to fabrication, assemblage and coupled out-of-plane dynamics. Nevertheless, we observe a good qualitative match between the low-order SDOF idealisation, Eq. (21), and experimental results.

Self-centring behaviour is observed in the system (experimental and numerical). In conventional seismic design of RC bridge piers, the pier structure can be subjected to residual tilting after the earthquake, due to large plastic deformation (plastic rotation at the base to dissipate energy). These features are important findings that are extremely useful for structures subject to earthquake loading.

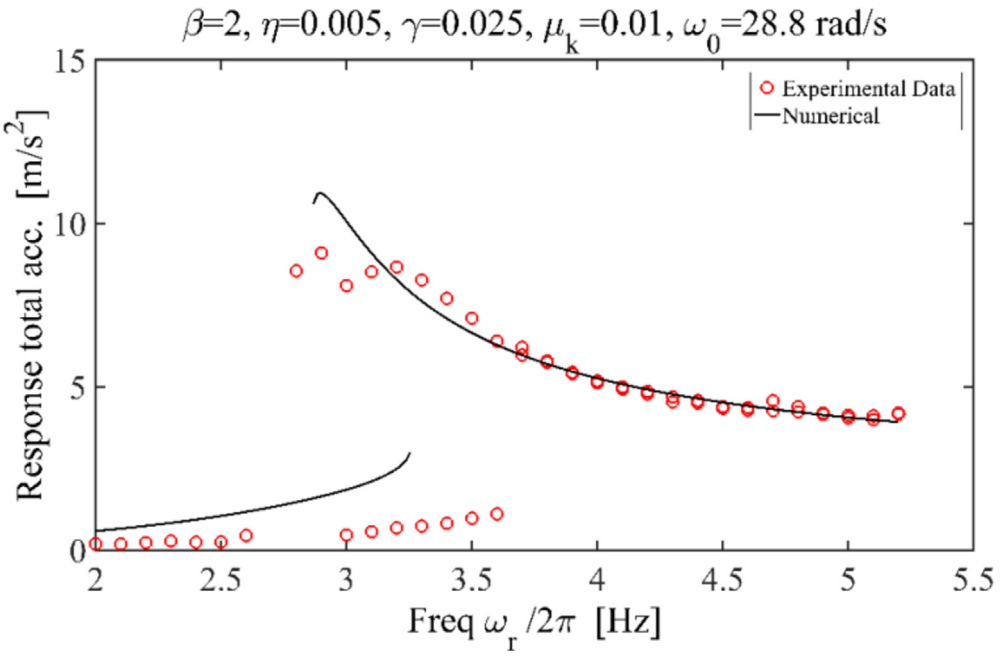

Fig. 9. Comparison of experimental and numerical nonlinear resonance curves for a 6 vertebrae column.

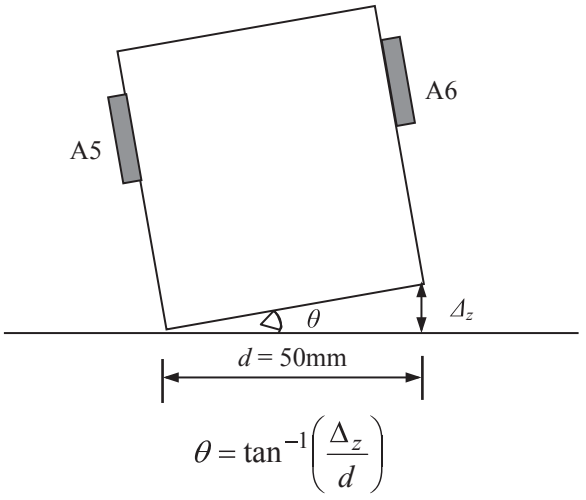

Fig. 10. Rotation of the first vertebrae due to rocking assuming a simplified SDOF model.

It should be noted that in the majority of cases, particularly for the systems with IRD, the total tip displacement of the structure will be larger than that found in this approximation (rigid body rotation assumption). In this case multiple joints open, with the largest opening typically still being at the base.

The total tip displacement of the column, calculated using the accelerometer data on top of the column, includes two components as shown in Fig. 13. In Fig. 13, Δ_{total}, is the overall total tip displacement of the column, δ_r is the tip displacement due to rocking of the base vertebra, and δ_f is the tip displacement due to the flexibility of the column (flexural deformation).

Fig. 14 shows the ratio of tip displacement due to rocking to the total tip displacement. Fig. 14 shows that the tip displacement of the column due to rocking is much higher for the column without IRD than the column with IRD. As discussed previously, this is due to the rigidity of the non-IRD column, causing it to rotate at the base, much like a conventional tied rigid rocking block problem. The addition of IRD in the structure adds more flexibility to all of the joints leading to horizontal displacements (included in the δ_f term). Therefore, although the energy dissipation is small, it occurs through deformation of

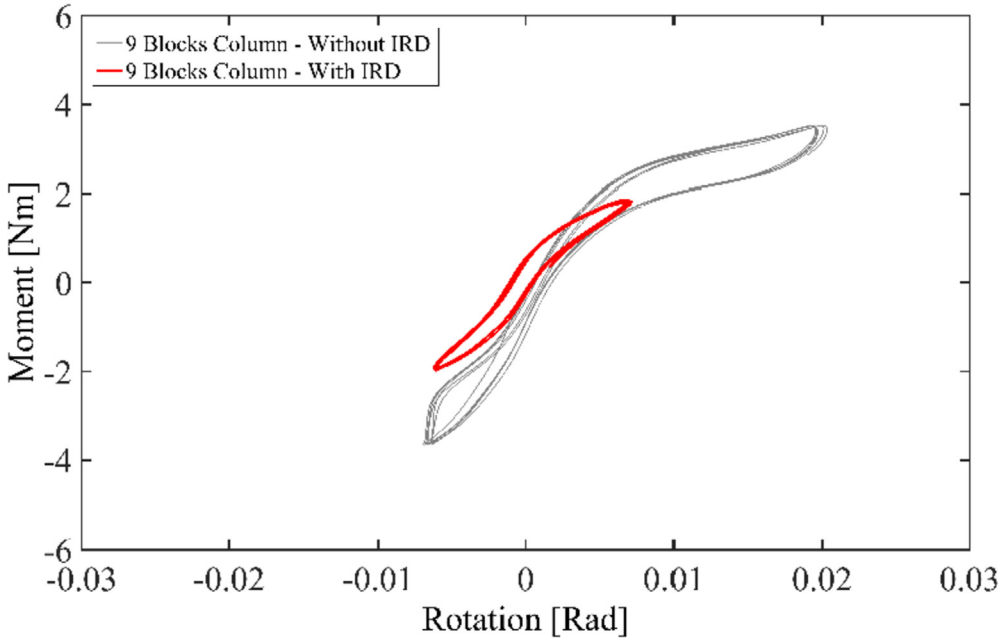

Fig. 11. Moment-rotation behaviour of 9 vertebrae column with and without IRD at displacement amplitude of 1.5 mm.

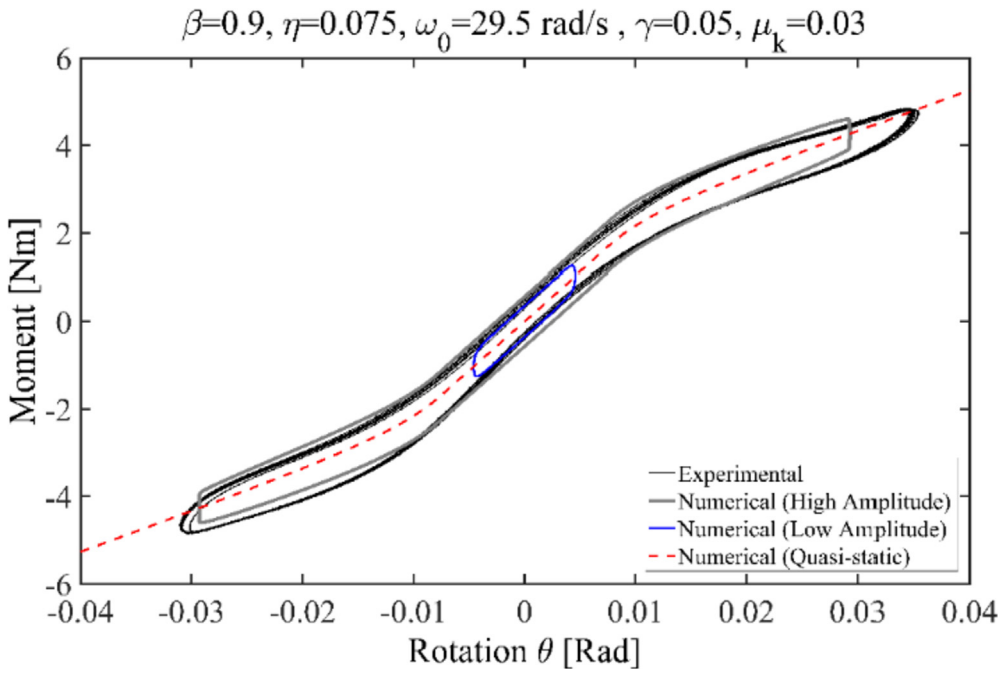

Fig. 12. Experimental, numerical quasi-static and dynamic moment-rotation graphs for 6 vertebrae column without IRD.

the rubber, added friction, and base rotation. Additionally, the spreading of 'point contact forces' (at the block edges) across the contact surface reduces the likelihood of a local bearing point failure of blocks.

With the derived numerical model, we can also estimate, numerically, the level of ground acceleration that will cause the structure to reach two critical limit states, namely 1% drift as serviceability limit state, and 4% drift for an ultimate failure limit state (where drift is the ratio of column tip displacement to column height). This is shown in Fig. 15, which is obtained from the stationary initial conditions $x(0) = \dot{x} = 0$. From a point (ω,A), the system is driven to a limit state. Below the boundary, the system has not reached the limit state, after an arbitrary (but reasonably long) time frame of 10s.

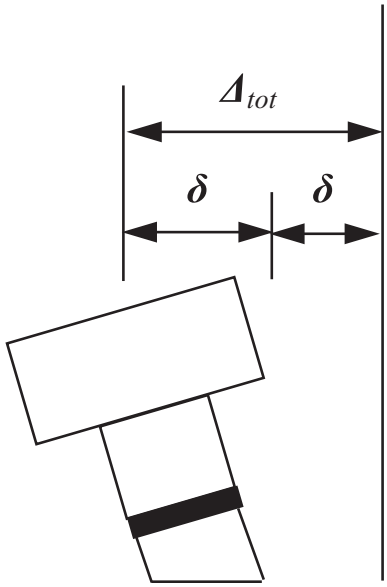

Fig. 13. Diagram showing how the total displacement is found.

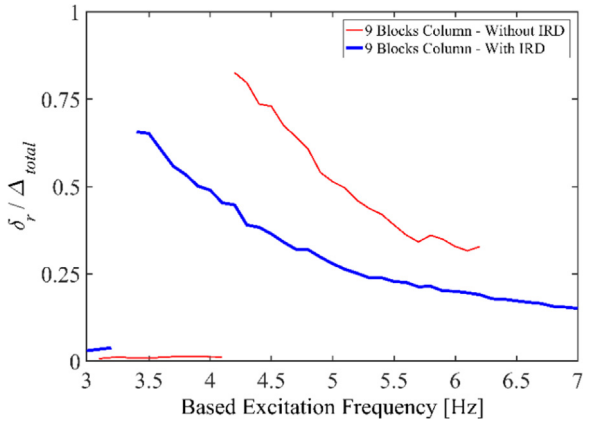

Fig. 14. Contribution of rocking motion in overall tip displacement of the column.

These figures however, do not tell the full story since we have assumed the structure starts from stationary initial conditions. With this assumption, we are favouring the steady state of the lower energy branches.

To find the initial conditions that are attracted to a steady-state solution for a given region of initial values, a grid of starts (GOS) can be used. This is a numerical technique that divides up the region of potential initial conditions into a grid. Each point of the grid is used as an initial condition and the steady-state response of the system is computed. Each starting point is plotted, usually as colour based on which steady-state solution is attracted [33]. Developing this strategy, the basins of attraction can be visualised. For example, in our particular case, for a ground acceleration of 0.15 g, the response of the system is shown in Fig. 16(a). In the range 3–5 Hz, two solutions coexist for the column without IRD. However, there is only one stable solution exists for the column with IRD. Fig. 16(b) shows the basins of attraction for 0.15 g ground excitation at 4 Hz. The red area corresponds to the basin of attraction of the low energy branch of the column without IRD. For these set of initial conditions, the response without IRD is smaller than the response with IRD. The grey area corresponds to the basin of attraction of the high energy solution, in this case the response without the IRD will be larger than the one with IRD.

In summary, the proposed system in this paper, shows a potential for a novel class of smart post-tensioned bridge piers, that can sustain large lateral displacement and deformation without experiencing any damage after the excitation. The challenge here is developing novel smart materials to replace the rubber to increase the energy dissipation capacity of the system. Alternatively, other means of energy dissipation techniques (e.g. semi-active dampers) can be implemented in this system, and rubber layers to be used to prevent the damage in solid vertebras. Once these problems are solved, the RC

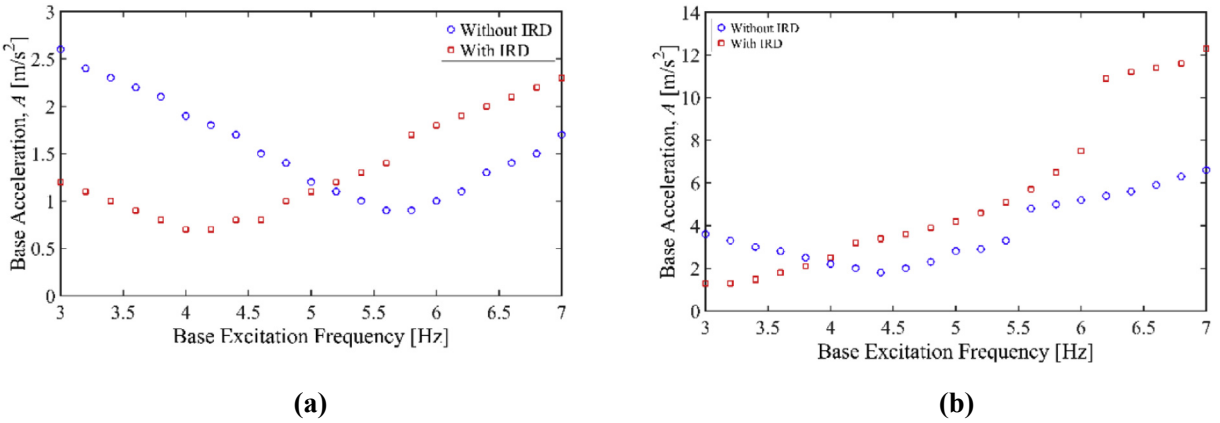

Fig. 15. Boundary for the system to reach the desired limit state: (a) 1% drift (serviceability limit state), and (b) 4% drift (ultimate failure limit state).

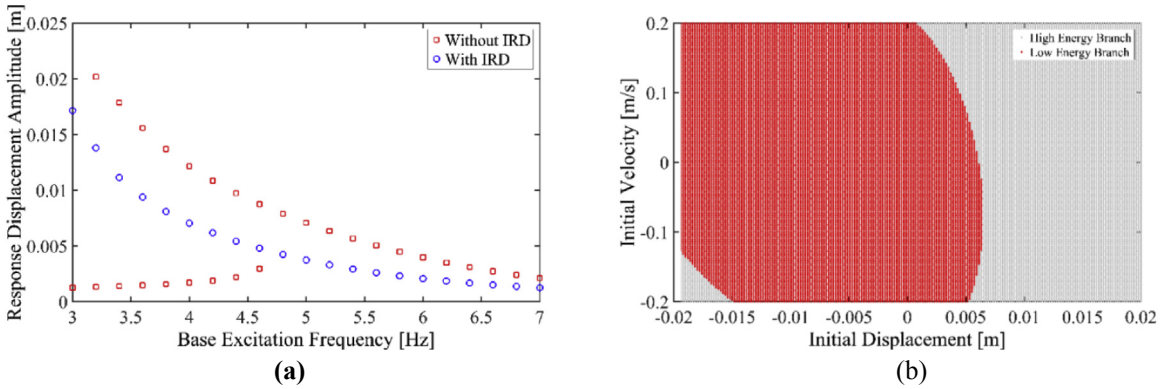

Fig. 16. Co-existing solutions for the system when is subjected to 0.15 g ground acceleration: (a) frequency sweeps [system without inserts presents co-existence of solutions], and (b) basin of attraction of the two coexisting solutions at 4 Hz.

materials for rigid vertebrae can be replaced with a more sustainable and durable material to reduce CO_2 emission, and eliminate corrosion problems, which has a significant impact on seismic fragility of RC structures [35,36]. In other words, since the vertebrae are essentially rigid blocks and only work in compression, there is no need to use conventional RC materials in bridge pier systems. This is a very important area for future research so that we can develop the next generation of accelerated bridge construction. The aim of this paper is to introduce this idea to the earthquake engineering and nonlinear dynamics research communities so that it can be developed in future research.

4. Conclusions

The nonlinear dynamics and mechanical behaviour of a proof of concept novel class of spinal bridge pier systems is explored experimentally. Two types of post-tensioned, unbounded spinal columns (a control without IRD, and the proposed model with IRD) with various heights are tested. The main outcomes of this research can be summarised as follows.

1. It is found that the inclusion of IRD results in a significant reduction in peak acceleration, for the high energy branch, and resonant frequency within the structures, at all heights due to increased flexibility at the joints.
2. The experimental results show no residual displacement in the spinal column system. This is due to the self-centring capability of the system, which is an important factor in seismic performance of bridge pier systems.
3. Adding IRD in the column improved the damping of the system by increasing the flexibility of the column and increasing the friction between the vertebrae.
4. The experimental results of the spinal columns without IRD show that the higher harmonics content in the response is increased by increasing the height of the column; i.e. a ‘higher modes effect’ is observed. However, adding IDR suppresses this effect.

5. The developed numerical reduced-order models permit the study of fold bifurcations structures that allow for co-existing high and low amplitude responses. The frequency interval over which these co-existing solutions occur (at a given forcing amplitude) is important to determine as it can increase design uncertainty as to peak system responses.
6. The proposed system in this paper, shows a potential for a novel class of smart post-tensioned bridge piers, which is able to withstand large amplitude cyclic dynamic loading without any damage. There is need for further research to improve the damping model of the system in the future. This is a very important area for future research so that we can develop the next generation of accelerated bridge construction.

Acknowledgements

The authors acknowledge support received by the UK Engineering and Physical Sciences Research Council (EPSRC) for the Engineering for a Prosperous Nation Grant [grant number EP/R039178/1: SPINE: Resilience-Based Design of Biologically Inspired Columns for Next-Generation Accelerated Bridge Construction].

References

[1] British Standards Institution, Eurocode 8: Design Provisions for Earthquake Resistance of Structures, British Standards Institution, London, 2004.
[2] Caltrans, Seismic Design Criteria. Caltrans VERSION 1.7, 2013.
[3] J.B. Mander, G.W. Rodgers, Analysis of low cycle fatigue effects on structures due to the 2010-2011 Canterbury earthquake sequence, in: Proceedings of the Tenth Pacific Conference on Earthquake Engineering, 2015. Sydney.
[4] K. Porter, K. Shaof, H. Seligson, Value of injuries in the Northridge earthquake, Earthq. Spectra 22 (2) (2006) 555–563.
[5] K. Kawashima, G. MacRae, J. Hoshikuma, K. Nagaya, Residual displacement response spectrum, J. Struct. Eng. 124 (5) (1998) 523–530.
[6] M.M. Kashani, Seismic Performance of Corroded RC Bridge Piers: Development of a Multi-mechanical Nonlinear Fibre Beam-column Model. PhD Thesis, University of Bristol, Bristol, 2014.
[7] M.M. Kashani, L.N. Lowes, A.J. Crewe, N.A. Alexander, Computational Modelling Strategies for Nonlinear Response Prediction of Corroded Circular RC Bridge Piers, 2016. https://doi.org/10.1155/2016/2738265.
[8] M. Ni Choine, M.M. Kashani, L.N. Lowes, A. O'Connor, A.J. Crewe, N.A. Alexander, J.E. Padgett, Nonlinear dynamic analysis and seismic fragility assessment of a corrosion damaged integral bridge, Int. J. Struct. Integr. 7 (2) (2016) 227–239.
[9] M.M. Kashani, A.J. Crewe, N.A. Alexander, Structural capacity assessment of corroded RC bridge piers, in: Proceedings of the Institution of Civil Engineers-bridge Engineering, 2017, pp. 1–14. https://doi.org/10.1680/jbren.15.00023.
[10] FHWA (Federal Highways Agency) HIF-12-013 2011 Accelerated Bridge Construction – Experience in Design, Fabrication and Erection of Prefabricated Bridge Elements and Systems – Final Manual. FHWA, McClean, VA, USA.
[11] Y.C. Ou, Precast Vertebral Post-tensioned Concrete Bridge Columns for Seismic Regions (Ph.D. Thesis), Dept. of Civil, Structural and Environmental Engineering, University of New York, Buffalo, United States of America, 2007.
[12] J.C. Lin, Y.L. Mo, The Shear Transfer Behavior of Precast Pre-stressed Hollow Rectangular Bridge Columns, National Cheng Kung University, Taiwan, Tainan, 2000.
[13] T. Arai, Y. Hishiki, K. Suda, T. Yamamoto, S. Takizawa, T. Onabe, Development of a New Precast Vertebral PC Pier, KaTRI Annual Report 48, KAJIMA Corporation, Japan, 2000.
[14] J.T. Hewes, M.J.N. Priestley, Seismic Design and Performance of Precast Concrete Vertebral Bridge Columns, Report No. SSRP–2001/25, Department of Structural Engineering, University of California, San Diego, 2002.
[15] S.L. Billington, J.K. Yoon, Cyclic response of unbonded posttensioned precast columns with ductile fiber-reinforced concrete, J. Bridge Eng. 9 (4) (2004) 353–363.
[16] S.L. Billington, J.K. Yoon, Cyclic response of unbonded posttensioned precast columns with ductile fiber-reinforced concrete, J. Bridge Eng. 9 (4) (2004) 353–363.
[17] D. Marriott, S. Pampanin, D. Bull, A. Palermo, Dynamic testing of precast, post-tensioned rocking wall systems with alternative dissipating solutions, Bull. N. Z. Soc. Earthq. Eng. 41 (2) (2008) 90–102.
[18] W.Y. Loo, C. Kun, P. Quenneville, N. Chouw, Experimental testing of a rocking timber shear wall with slip-friction connectors, Earthq. Eng. Struct. Dynam. 43 (11) (2014) 1621–1639.
[19] J.C. Wang, Y.C. Ou, K.C. Chang, G.C. Lee, Large-scale seismic tests of tall concrete bridge columns with precast segmental construction, Earthq. Eng. Struct. Dynam. 37 (12) (2008) 1449–1465.
[20] J.B. Mander, C.T. Cheng, Seismic Resistance of Bridge Piers Based on Damage Avoidance Design, Technical Report, NCEER 97-0014, National Center of Earthquake Engineering Research, Buffalo, New York, 1997.
[21] P. Sideris, Nonlinear quasi-static analysis of hybrid sliding-rocking bridge columns subjected to lateral loading, Eng. Struct. 101 (2015) 125–137.
[22] I. Stokes, D.M. Greenapple, Measurement of surface deformation of soft tissue, J. Biomech. 18 (1) (1985) 1–7. https://doi.org/10.1016/0021-9290(85)90040-5.
[23] M.S. Williams, A. Blakeborough, Laboratory testing of structures under dynamic loads: an introductory review, Phil. Trans. Roy. Soc. Lond. A 359 (2001) 1651–1669. https://doi.org/10.1098/rsta.2001.0860.
[24] N. Ogawa, K. Ohtani, T. Katayama, H. Shibata, Construction of a three-dimensional, large-scale shaking table and development of core technology, Phil. Trans. Roy. Soc. Lond. A 359 (2001) 1725–1751. https://doi.org/10.1098/rsta.2001.0871.
[25] Quijano N., Passino K. A tutorial introduction to control systems development and implementation with dSPACE. http://www.ece.osu.edu/_passino/dSPACEtutorial.doc.pdf.
[26] N. Alexander, O. Oddbjornsson, C. Taylor, H. Osinga, D. Kelly, Exploring the dynamics of a class of post-tensioned, moment resisting frames, J. Sound Vib. 330 (15) (2011) 3710–3728. http://.dx.doi.org/10.1016/j.jsv.2011.02.016.
[27] A.H. Nayfeh, D.T. Mook, Nonlinear Oscillations, Wiley-Interscience, New York, 1979.
[28] G. Kerschen, K. Worden, A.F. Vakakis, J.C. Golinval, Past, present and future of nonlinear system identification in structural dynamics, Mech. Syst. Signal Process. 20 (2006) 505–592. https://doi.org/10.1016/j.ymssp.2005.04.008.
[29] K. Worden, G.R. Tomlinson, Nonlinearity in Structural Dynamics: Detection, Identification and Modelling, Institute of Physics Publishing, Bristol and Philadelphia, 2001. ISBN 10: 7111393864.
[30] O. Oddbjornsson, Dynamics of Nonlinear Elastic Moment Resisting Frames. PhD Thesis, University of Bristol, Bristol, 2009.
[31] R.J. Kuether, L. Renson, T. Detroux, C. Grappasonni, G. Kerschen, M.S. Allen, Nonlinear normal modes, model interactions and isolated resonances curves, J. Sound Vib. 351 (2015) 299–310.
[32] R.M. Rosenberg, Normal modes of nonlinear dual-mode systems, J. Appl. Mech. 27 (1960) 263–368.
[33] D. Wagg, S. Neild, Nonlinear Vibration with Control, Springer, 2014. ISBN 978-90-481-2836-5.

[34] H. Roh, A. Reinhorn, Hysteretic behaviour of precast vertebral bridge piers with superelastic shape memory alloy bars, Eng. Struct. 32 (10) (2010) 3394–3403.
[35] M. Ni Choine, M.M. Kashani, L.N. Lowes, A. O'Connor, A.J. Crewe, N.A. Alexander, J.E. Padgett, Nonlinear dynamic analysis and seismic fragility assessment of a corrosion damaged integral bridge, Int. J. Struct. Integr. 7 (2) (2016) 227–239.
[36] E. Afsar Dizaj, R. Madandoust, M.M. Kashani, Exploring the impact of chloride-induced corrosion on seismic damage limit states and residual capacity of reinforced concrete structures, Struct. Infrastruct. Eng. 14 (6) (2017) 714–729.